East European Journal of Physics. **2.** 121-129 (2024)
DOI:10.26565/2312-4334-2024-2-10 ISSN 2312-4334

EVOLUTION OF VECTOR VORTEX BEAMS FORMED BY A TERAHERTZ LASER METAL RESONATOR

Andrey V. Degtyarev, Mykola M. Dubinin, Vyacheslav A. Maslov*, Konstantin I. Muntean, Oleh O. Svystunov
V.N. Karazin Kharkiv National University, 4 Svoboda Sq., Kharkiv 61022, Ukraine
**Corresponding Author*: *v.a.maslov@karazin.ua*
Received February 8, 2024; revised March 31, 2024; accepted April 8, 2024

Analytical expressions for the nonparaxial mode diffraction of a terahertz laser metal waveguide resonator are obtained. The study assumes interaction between the modes and a spiral phase plate, considering different topological charges (n). Also, using numerical modeling, the physical features of the emerging vortex beams as they propagate in free space are studied. The Rayleigh-Sommerfeld vector theory is employed to investigate the propagation of vortex laser beams in the Fresnel zone, excited by the modes of a metal waveguide quasi-optical resonator upon incidence on a spiral phase plate. In free space, the spiral phase plate for exciting TE_{11} mode from the profile with the intensity maximum in the center (n = 0) forms an asymmetric ring one with two maxima (n = 1, 2). For the exciting TE_{01} mode, the initial ring (n = 0) structure of the field intensity is transformed into a structure with a maximum radiation intensity in the center (n = 1), and later again into a ring (n = 2). The phase front of the beam for the E_y component of the linearly polarized along the y axis TE_{11} mode changes from spherical to spiral with one on-axis singularity point. In the phase profile of the transverse components of the azimuthally polarized TE_{01} mode, a region with two and three off-axis phase singularity points appears.
Keywords: *Terahertz laser; Metal waveguide resonator; Spiral phase plate; Vortex beams; Polarization; Radiation propagation*
PACS: 42.55.Lt; 42.60.Da; 42.25.Bs; 47.32.C–

INTRODUCTION

In the past decade, there has been a notable surge in interest regarding the formation of terahertz laser beams [1]. Vortex beams within these wave fields hold a prominent position in research. Their uniqueness stems from the distinct spiral structure of the wavefront, ensuring the presence of an orbital wave momentum with a considerable number of states and, consequently, additional degrees of freedom [2 – 4]. Vortex laser beams demonstrate significant potential for applications in high-speed multiplex terahertz communication systems, tomography, the exploration of linear and nonlinear material responses, the acceleration and manipulation of electron bunches, and the detection of astrophysical sources [5 – 9].

The study of THz vortex beam generation primarily focuses on two principles: wavefront modulation through specialized external devices and direct excitation of vortex beams at the output of the resonator. The extracavity wavefront modulation principle employs various tools such as spiral phase plates, q-plates, achromatic polarization elements, diffractive optical elements, metasurfaces, liquid crystal branched polarization gratings, computer holograms, and spatial modulators [10 – 17]. Techniques like optical rectification, difference-frequency generation, and laser-plasma methods have been proposed for forming vortex beams at the laser resonator output [18 – 20]. However, the majority of these studies utilize broadband radiation from subpicosecond pulse generators based on femtosecond lasers, leading to the complex manufacturing of laser systems and interactions with matter that significantly deviate from continuous radiation.

Optically pumped molecular lasers stand out as the sole compact source of continuous terahertz radiation, offering discrete tunability across the entire terahertz range and boasting a narrow spectral linewidth. The current surge in interest for these generators is attributed to the potential use of continuously tunable mid-IR quantum cascade lasers as pump sources [21]. The utilization of metal waveguide quasi-optical resonators is common in most optically pumped lasers, enabling the achievement of relatively high powers (up to 1 W) in a continuous regime with relatively compact cavity sizes [22]. Among the modes of such resonators, TE_{11} and TE_{01} modes with linear and azimuthal polarization exhibit the lowest losses [23].

One of the most renowned optical elements for generating vortex beams is the spiral phase plate with azimuthally varying thickness [3, 24]. This element enables the direct application of a spiral phase shift to the incident laser beam, converting almost 100 % of the incoming radiation energy into a vortex beam.

This study aims to derive analytical expressions that describe the nonparaxial diffraction of modes a metal waveguide resonator of a terahertz laser when interacting with a spiral phase plate. Additionally, through numerical simulations, the research investigates the physical characteristics of the resulting vortex beams during their propagation in free space.

Cite as: A.V. Degtyarev, M.M. Dubinin, V.A. Maslov, K.I. Muntean, O.O. Svystunov, East Eur. J. Phys. 2, 121 (2024), https://doi.org/10.26565/2312-4334-2024-2-10
© A.V. Degtyarev, M.M. Dubinin, V.A. Maslov, K.I. Muntean, O.O. Svystunov, 2024; CC BY 4.0 license

THEORETICAL RELATIONSHIPS

The well-known vectorial Rayleigh-Sommerfeld integrals in the Cartesian coordinate system will be employed to describe the propagation of laser radiation in free space along the 0*z* axis [25 – 27]:

$$\begin{aligned} E_x(\vec{r}) &= -\frac{1}{2\pi}\int\limits_{\Sigma_0}\int E_x^0(\vec{r}_0)\frac{\partial}{\partial z}\left[\frac{\exp(ikR)}{R}\right]dx_0dy_0, \\ E_y(\vec{r}) &= -\frac{1}{2\pi}\int\limits_{\Sigma_0}\int E_y^0(\vec{r}_0)\frac{\partial}{\partial z}\left[\frac{\exp(ikR)}{R}\right]dx_0dy_0, \\ E_z(\vec{r}) &= \frac{1}{2\pi}\int\limits_{\Sigma_0}\int\left\{E_x^0(\vec{r}_0)\frac{\partial}{\partial x}\left[\frac{\exp(ikR)}{R}\right]+E_y^0(\vec{r}_0)\frac{\partial}{\partial y}\left[\frac{\exp(ikR)}{R}\right]\right\}dx_0\,dy_0, \end{aligned} \tag{1}$$

where $E_x^0(\vec{r}_0)$ and $E_y^0(\vec{r}_0)$ are the complex amplitudes of the *x* and *y* components of the input electric field, Σ_0 is the area in which the input field is specified, $k = 2\pi/\lambda$ is the wave number, λ is the wavelength, $\vec{r}_0 = x_0\,\vec{e}_{x_0} + y_0\,\vec{e}_{y_0}$, (x_0, y_0) are the Cartesian coordinates in the source plane, $\vec{r} = x\vec{e}_x + y\vec{e}_y + z\vec{e}_z$, (x, y, z) are the Cartesian coordinates in the observation plane, $R = \sqrt{(x-x_0)^2 + (y-y_0)^2 + z^2}$. Using nonparaxial approximation (1), let us expand *R* into a series, keeping its first and second terms in the form

$$R \cong r + \frac{x_0^2 + y_0^2 - 2xx_0 - 2yy_0}{2r}, \tag{2}$$

where $r = \sqrt{x^2 + y^2 + z^2}$.

Substituting (2) into the integrand, which includes rapidly oscillating exponents (1), and at other positions $R \cong r$, and then transitioning to cylindrical coordinates, yields expressions for the field components in different diffraction zones:

$$E_x(\rho,\beta,z) = -\frac{iz}{\lambda r^2}\exp(ikr)\int_0^\infty\int_0^{2\pi} E_x^0(\vec{r}_0)\exp\left(ik\frac{\rho_0^2}{2r}\right)\exp\left(-ik\frac{\rho\rho_0\cos(\varphi-\beta)}{r}\right)\rho_0 d\rho_0 d\varphi, \tag{3.1}$$

$$E_y(\rho,\beta,z) = -\frac{iz}{\lambda r^2}\exp(ikr)\int_0^\infty\int_0^{2\pi} E_y^0(\vec{r}_0)\exp\left(ik\frac{\rho_0^2}{2r}\right)\exp\left(-ik\frac{\rho\rho_0\cos(\varphi-\beta)}{r}\right)\rho_0 d\rho_0 d\varphi, \tag{3.2}$$

$$\begin{aligned} E_z(\rho,\beta,z) = \frac{i}{\lambda r^2}\exp(ikr)\int_0^\infty\int_0^{2\pi}&\left[E_x^0(\vec{r}_0)(\rho\cos\beta-\rho_0\cos\varphi)+E_y^0(\rho\sin\beta-\rho_0\sin\varphi)\right] \\ &\times\exp\left(ik\frac{\rho_0^2}{2r}\right)\exp\left(-ik\frac{\rho\rho_0\cos(\varphi-\beta)}{r}\right)\rho_0\,d\rho_0\,d\varphi. \end{aligned} \tag{3.3}$$

Here (ρ,β,z) are cylindrical coordinates in the observation plane and (ρ_0,φ) are the polar coordinates in the area where the input field is specified, $r = \sqrt{\rho^2 + z^2}$.

Investigated metal waveguide resonator modes coincide with the modes of a circular metal waveguide. Hence, in the initial plane, we characterize radiation through linearly and azimuthally polarized waveguide TE_{11} and TE_{01} modes. The normalized Cartesian components of electromagnetic fields for these modes take the following form in the source plane ($z = 0$) [28]:

$$\text{TE}_{11}\text{ mode}\begin{cases} E_x^0(\rho_0,\varphi) = A_{11}J_2(\chi_{11}\dfrac{\rho_0}{a})\sin(2\varphi), \\ E_y^0(\rho_0,\varphi) = A_{11}[J_0(\chi_{11}\dfrac{\rho_0}{a}) - J_2(\chi_{11}\dfrac{\rho_0}{a})\cos(2\varphi)], \end{cases} \tag{4}$$

$$\text{TE}_{01}\text{ mode}\begin{cases} E_x^0(\rho_0,\varphi) = -A_{01}J_1(\chi_{01}\dfrac{\rho_0}{a})\,\sin(\varphi), \\ E_y^0(\rho_0,\varphi) = A_{01}J_1(\chi_{01}\dfrac{\rho_0}{a})\,\cos(\varphi), \end{cases} \tag{5}$$

where a is the waveguide radius, $A_{11} = \dfrac{\chi_{11}}{\left(a J_1(\chi_{11})\sqrt{2\pi\left(\chi_{11}^2 - 1\right)}\right)}$, $A_{01} = \dfrac{1}{a\sqrt{\pi} J_0(\chi_{01})}$ are the normalizing factors, J_j is the Bessel function of the 1st kind of order j; χ_{mn} is the n-th root of the equation $J_m(\chi) = 0$.

We will explore the interaction between these modes and a spiral phase plate (SPP) with arbitrary topological charge (n) [29]. The SPP is positioned at the output of a waveguide with an aperture of the same diameter, as illustrated in Figure 1. The complex transmission function of an SPP with a radius a is expressed in polar coordinates as follows [3]:

$$T_n(\rho_0, \varphi) = \mathrm{circ}\left(\frac{\rho_0}{a}\right)\exp(in\varphi), \tag{6}$$

where $\mathrm{circ}(\cdot)$ is the circular function.

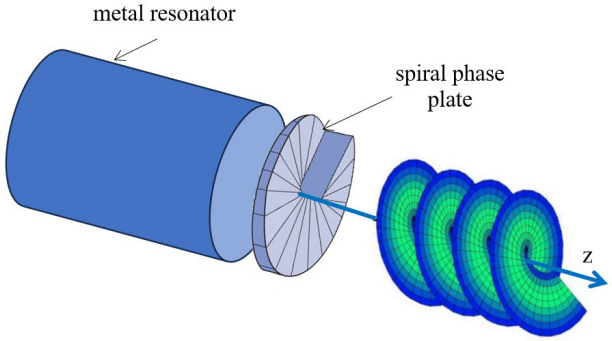

Figure 1. Topology of the model.

For simplifying calculations, integration over the angle φ in equation (3) can be carried out using the established relations for the integer $m \geq 0$, as described in [26]:

$$\int_0^{2\pi} \cos(m\varphi + \varphi_0)\exp[-ix\cos(\varphi - \theta)d\varphi = 2\pi(-i)^m J_m(x)\cos(m\theta + \varphi_0),$$

$$\int_0^{2\pi} \sin(m\varphi + \varphi_0)\exp[-ix\cos(\varphi - \theta)d\varphi = 2\pi(-i)^m J_m(x)\sin(m\theta + \varphi_0).$$

Then from here we can obtain the following relation

$$\int_0^{2\pi} e^{-ix\cos(\varphi-\beta)} e^{in\varphi} d\varphi = 2\pi e^{in\beta}(-i)^n J_n(x)\,. \tag{7}$$

Using Euler's formulas for the trigonometric functions and taking into account Eq. (7), we obtain the expressions for the following integrals:

$$\int_0^{2\pi} e^{-ix\cos(\varphi-\beta)} e^{in\phi}\sin(m\varphi + \varphi_0)\,d\varphi = \frac{\pi}{i}\{e^{i[(n+m)\beta+\varphi_0]}(-i)^{n+m} J_{n+m}(x) - e^{i[(n-m)\beta-\varphi_0]}(-i)^{n-m} J_{n-m}(x)\}, \tag{8.1}$$

$$\int_0^{2\pi} e^{-ix\cos(\varphi-\beta)} e^{in\varphi}\cos(m\varphi + \varphi_0)\,d\varphi = \pi\{e^{i[(n+m)\beta+\varphi_0]}(-i)^{n+m} J_{n+m}(x) + e^{i[(n-m)\beta+\varphi_0]}(-i)^{n-m} J_{n-m}(x)]\,. \tag{8.2}$$

Then, substituting into (3) the expression for the complex transmission function of the SPP (6) and using formulas (7) and (8.1), we obtain expressions for the field components that describe the nonparaxial diffraction of the TE_{11} mode by the SPP with topological charge n in free space:

$$E_x(\rho, \beta, z) = \frac{(-i)^n kz}{2r^2}\exp[i(n\beta + kr)]\,A_{11}[\exp(i2\beta)H1_{2,n+2}(\rho, z) - \exp(-i2\beta)H1_{2,n-2}(\rho, z)], \tag{9.1}$$

$$E_y(\rho,\beta,z)=\frac{(-i)^{n+1}kz}{r^2}\exp[i(n\beta+kr)]\,A_{11}[H1_{0,n}(\rho,z) + \frac{1}{2}[\exp(i2\beta)H1_{2,n+2}(\rho,z)+\exp(-i2\beta)H1_{2,n-2}(\rho,z)], \tag{9.2}$$

$$E_z(\rho,\beta,z)=\frac{(-i)^{n+1}k}{2r^2}\exp[i(n\beta+kr)]\;A_{11}\,[G1(\rho,\beta,z)+G2(\rho,\beta,z) + 2\rho\sin(\beta)H1_{0,n}(\rho,z)], \tag{9.3}$$

where the following notations are introduced

$$H1_{0,n}(\rho,z)=\int_0^a J_0\left(\chi_{11}\frac{\rho_0}{a}\right)\exp\left(ik\frac{\rho_0^2}{2r}\right)J_n\left(\frac{k\rho\rho_0}{r}\right)\rho_0 d\rho_0, \tag{10.1}$$

$$H1_{2,n}(\rho,z)=\int_0^a J_2\left(\chi_{11}\frac{\rho_0}{a}\right)\exp\left(ik\frac{\rho_0^2}{2r}\right)J_n\left(\frac{k\rho\rho_0}{r}\right)\rho_0 d\rho_0, \tag{10.2}$$

$$G1(\rho,\beta,z)=\int_0^a J_2\left(\chi_{11}\frac{\rho_0}{a}\right)\exp\left(ik\frac{\rho_0^2}{2r}\right) \times\left[\exp(i\beta)J_{n-2}\left(\frac{k\rho\rho_0}{r}\right)-\exp(-i\beta)J_{n+2}\left(\frac{k\rho\rho_0}{r}\right)\right]\rho_0 d\rho_0, \tag{10.3}$$

$$G2(\rho,\beta,z)=\int_0^a\left[J_0\left(\chi_{11}\frac{\rho_0}{a}\right)+J_2\left(\chi_{11}\frac{\rho_0}{a}\right)\right]\exp\left(ik\frac{\rho_0^2}{2r}\right) \times\left[\exp(i\beta)J_{n+1}\left(\frac{k\rho\rho_0}{r}\right)-\exp(-i\beta)J_{n-1}\left(\frac{k\rho\rho_0}{r}\right)\right]\rho_0^2 d\rho_0. \tag{10.4}$$

Also, using formulas (8.1) and (8.2), we obtain expressions for the field components that describe the nonparaxial diffraction of the TE_{01} mode on the SPP. They look as follows:

$$E_x(\rho,\beta,z)=\frac{(-i)^{n+1}k\,z}{2r^2}\exp[i(n\,\beta+kr)]\,B_{01}\left[\exp(i\beta)\,H2_{1,n+1}(\rho,z)+\exp(-i\beta)\,H2_{1,n-1}(\rho,z)\right], \tag{11.1}$$

$$E_y(\rho,\beta,z)=\frac{(-i)^{n+2}kz}{2r^2}\exp[i(n\,\beta+kr)]\,B_{01}\left[\exp(i\beta)\,H2_{1,n+1}(\rho,z)-\exp(-i\beta)\,H2_{1,n-1}(\rho,z)\right], \tag{11.2}$$

$$E_z(\rho,\beta,z)=\frac{(-i)^{n+1}k\rho}{2r^2}\exp[i(n\,\beta+kr)]\,B_{01}[H2_{1,n+1}(\rho,z)+H2_{1,n-1}(\rho,z)], \tag{11.3}$$

where the following notation is introduced

$$H2_{1,n}(\rho,z)=\int_0^a J_1\left(\chi_{01}\frac{\rho_0}{a}\right)\exp\left(ik\frac{\rho_0^2}{2r}\right)J_n\left(\frac{k\rho\rho_0}{r}\right)\rho_0 d\rho_0.$$

NUMERICAL RESULTS AND DISCUSSIONS

Using the obtained expressions, calculations of the longitudinal and transverse distributions of the total field intensity were carried out. ($I=\left|E_x\right|^2+\left|E_y\right|^2+\left|E_z\right|^2$), as well as transverse intensity distributions ($I=\left|E_i\right|^2$, $i=x,y$) and phases ($\varphi=\mathrm{arctg}(\mathrm{Im}(E_i)/\mathrm{Re}(E_i))$) fields for individual *x*, *y* components of laser radiation beams excited in the Fresnel zone by an asymmetrical linearly polarized along the *y* axis TE_{11} mode and a symmetrical azimuthally polarized TE_{01} mode of a metal waveguide resonator of a terahertz laser during their interaction with the SPP. The transverse distributions of the field intensity and phase for the longitudinal component are not given due to its insignificant influence on the total radiation intensity. The radiation wavelength was chosen in the middle part of the terahertz range $\lambda = 0.4326$ mm (the lasing line of optically excited formic acid molecule HCOOH [30]). The waveguide diameter is chosen to be $2a = 35$ mm. The SPP with an aperture of the same diameter was placed at the output of the waveguide. In this case, the topological charge *n* changed from zero to two.

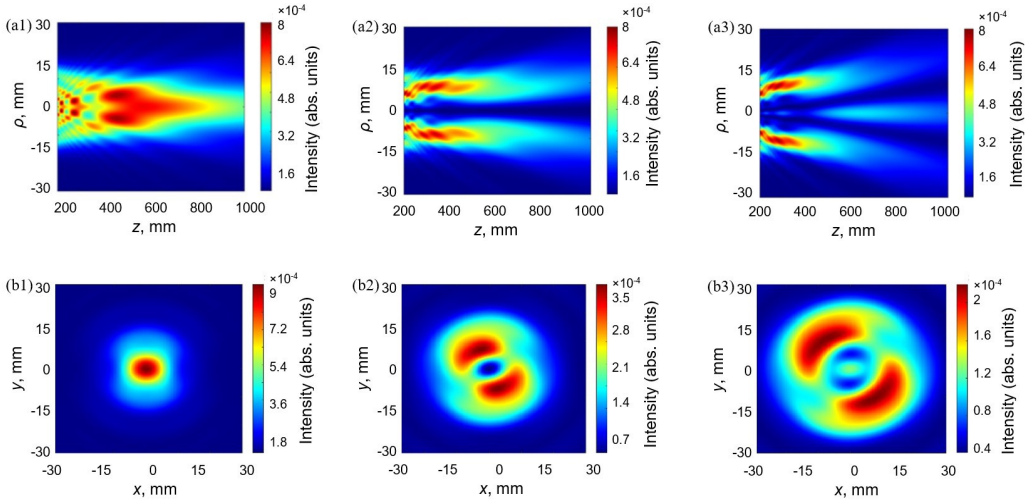

Figure 2. Calculated longitudinal (a1–a3) and transverse (b1–b3) total field intensity distributions of the laser beams excited by the TE_{11} mode in the Fresnel zone for different values of the topological charge. The first, second and third columns correspond to $n = 0$, $n = 1$ and $n = 2$, respectively.

Figure 2 (a1), 2(b1) show the results of numerical simulation for the longitudinal intensity field distribution in the Fresnel zone ($z = 100 - 1000$ mm) and the transverse intensity field distribution excited by the TE_{11} mode for $z = 708$ mm (where the Fresnel number is 1). The results were obtained under the assumption that there is no SPP at the waveguide output. One can observe from the figures that the maximum in the distribution of longitudinal intensity is observed at $z \approx 500$ mm. Notice that the effective beam diameter at a distance of 708 mm for the TE_{11} mode is calculated according to the formula [31]

$$d_\sigma = 2\sqrt{\frac{2\int_0^{2\pi}\int_0^{\infty}\rho^2 I(\rho,\beta,z)\,\rho\,d\rho\,d\beta}{\int_0^{2\pi}\int_0^{\infty} I(\rho,\beta,z)\,\rho\,d\rho\,d\beta}}$$

and is equal to $d_\sigma = 151.3\ \lambda$. The transverse field profile has a well-known Gaussian-like shape and a spherical phase front. Installing a SPP at the output of a waveguide with a non-zero topological charge leads in the Fresnel zone to a change in the beam intensity profile to an asymmetric annular one with two maxima (Figure 2 (a2, a3, b2, b3)). The beam diameter increases to $d_\sigma = 164.6\ \lambda$ at $n = 1$ and $d_\sigma = 192.0\ \lambda$ at $n = 2$.

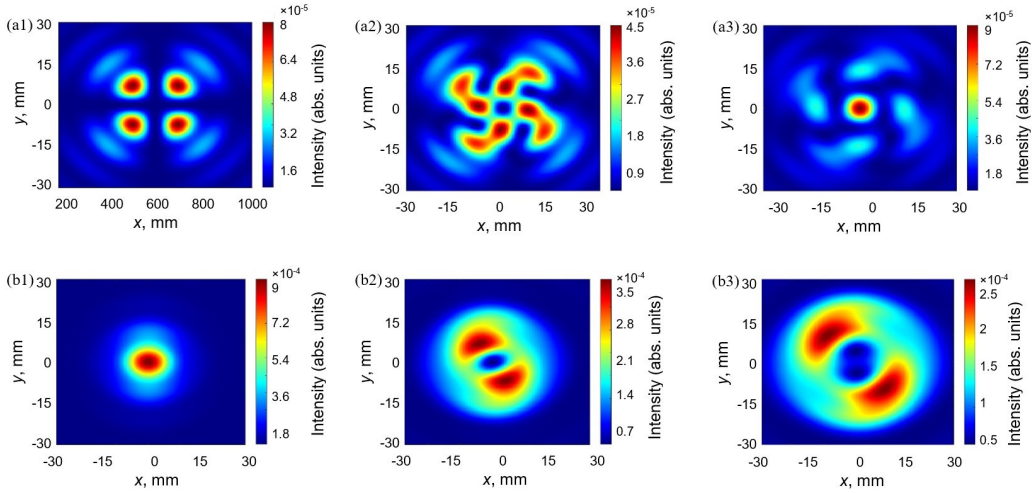

Figure 3. Calculated field intensity distributions for E_x (a1–a3) and E_y (b1–b3) components of the laser beams excited by the TE_{11} mode in the Fresnel zone for different values of the topological charge. The first, second and third columns correspond to $n = 0$, $n = 1$ and $n = 2$, respectively.

Figures 3–4 show the calculated distributions of field intensity and phase for individual transverse components excited in the Fresnel zone by an asymmetric linearly polarized along the y axis TE_{11} mode of a metal waveguide

resonator of a terahertz laser during its interaction with the SPP. These results clearly demonstrate the determining role of the E_y component of the laser beam in the formation of the total transverse intensity profile in Figure 2. Note the observed focusing of the field intensity of the E_x-component of the laser beam in the case of an increase in the value of the topological charge.

As can be seen from Figure 4, the installation of the SPP at the output of the waveguide for the TE_{11} mode leads to the transformation of the beam phase profile from spherical to vortex. In this case, with an increase in the value of the topological charge, the formation of a pronounced helical structure of the wave front and a singularity point for the E_y component of the laser beam is observed.

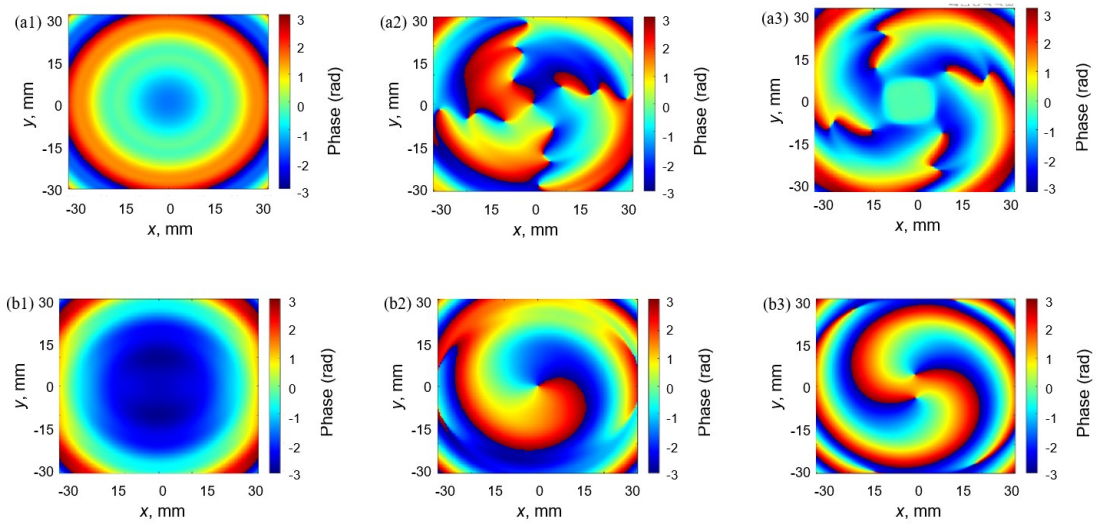

Figure 4. Calculated field phase distributions for E_x (a1–a3) and E_y (b1–b3) components of the laser beams excited by the TE_{11} mode in the Fresnel zone for different values of the topological charge. The first, second and third columns correspond to $n = 0$, $n = 1$ and $n = 2$, respectively.

The installation of the SPP at the output of the waveguide for the TE_{01} mode leads to the transformation of the beam intensity profile from annular to Gaussian-like when the value of the topological charge changes from zero to one (Figure 5). Further increase in the topological charge returns the beam profile to its original annular shape. Mention that the beam diameter at a distance of 708 mm for the TE_{01} mode increases from $d_\sigma = 67.5\ \lambda$ at $n = 0$ (in the absence of topological charge) to $d_\sigma = 89.1\ \lambda$ at $n = 2$.

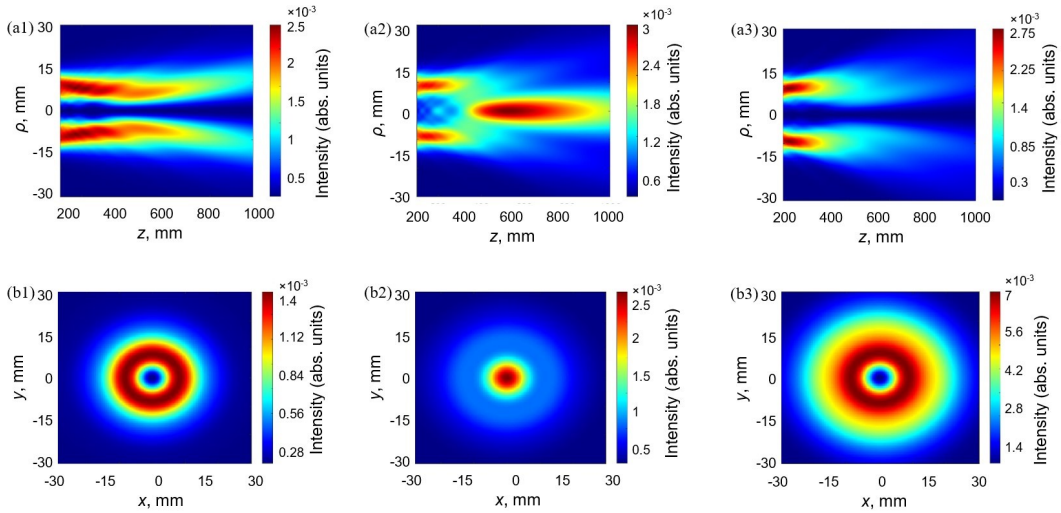

Figure 5. Calculated longitudinal (a1–a3) and transverse (b1–b3) total field intensity distributions excited by the TE_{01} mode in the Fresnel zone for different values of the topological charge. The first, second and third columns correspond to $n = 0$, $n = 1$ and $n = 2$, respectively.

Figure 6 shows the calculated transverse field intensity distributions for individual transverse components of laser radiation beams excited in the Fresnel zone by a symmetrical azimuthally polarized TE_{01} mode of a metal waveguide resonator of a terahertz laser during its interaction with the SPP. These results show the same contribution of the transverse components of the laser beam to the formation of the total intensity profile in Figure 5. Possessing an initially antisymmetric shape, these components, when added, form a symmetrical beam.

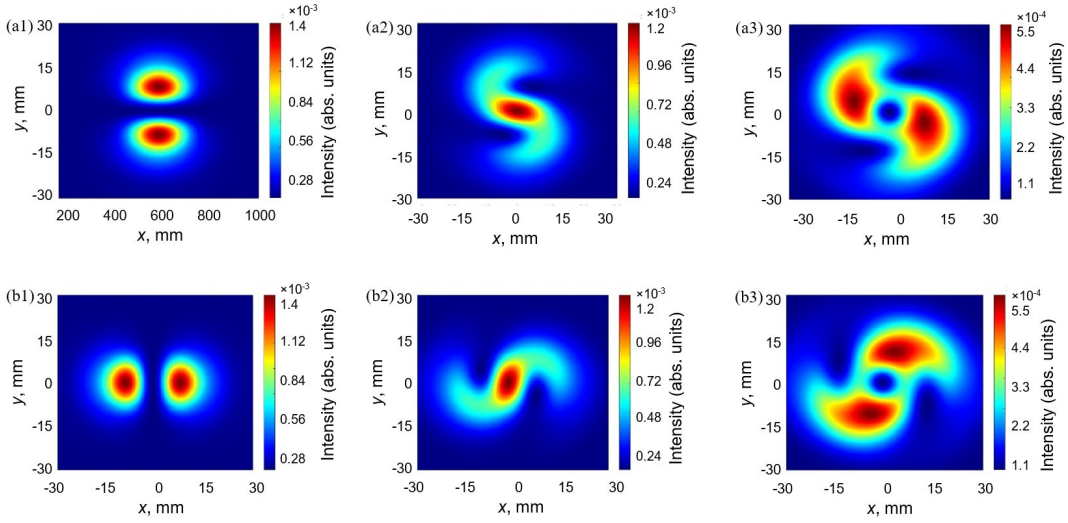

Figure 6. Calculated field intensity distributions for E_x (a1–a3) and E_y (b1–b3) components of the laser beams excited by the TE_{01} mode in the Fresnel zone for different values of the topological charge. The first, second and third columns correspond to $n = 0$, $n = 1$ and $n = 2$, respectively.

Figure 7 shows the phase distributions for the transverse components of the TE_{01} mode in the Fresnel zone when the topological charge changes. Installing the SPP at the output of the waveguide, as for the TE_{11} mode, converts the wavefront of laser beams from spherical to vortex. Note that for $n = 1$ the wavefront has two helical surfaces, and for $n = 2$ it has three.

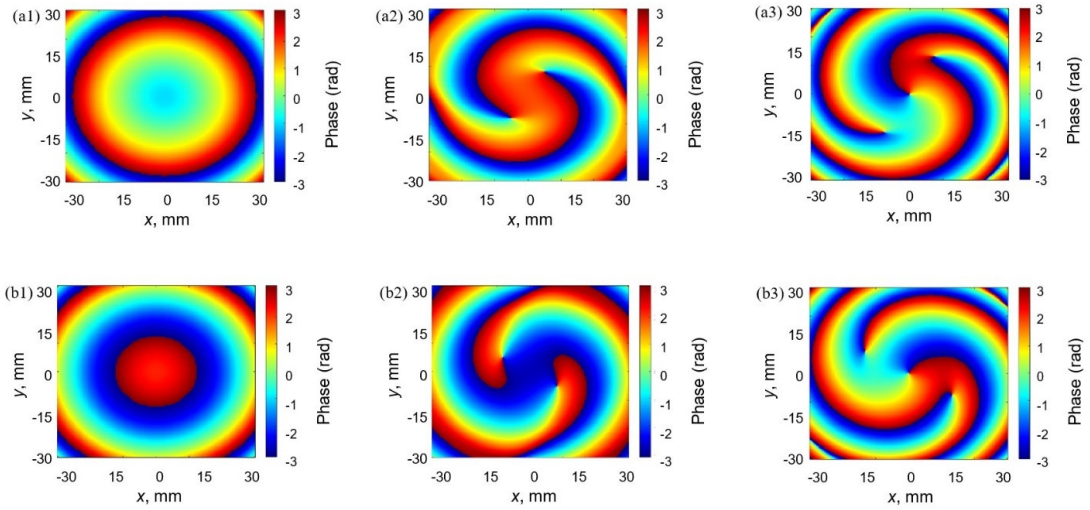

Figure 7. Calculated field phase distributions for E_x (a1–a3) and E_y (b1–b3) components of the laser beams excited by the TE_{01} mode in the Fresnel zone for different values of the topological charge. The first, second and third columns correspond to $n = 0$, $n = 1$ and $n = 2$, respectively.

CONCLUSIONS

Analytical expressions have been obtained to describe the nonparaxial diffraction of modes of a metal waveguide resonator of a terahertz laser during their interaction with a spiral phase plate with different topological charges (n). The determining role of the E_y component of the laser beam for the exciting linearly polarized along the y axis TE_{11} mode and the equal contribution of the transverse components for the exciting azimuthally polarized TE_{01} mode in the formation of the total transverse field are shown.

In free space, the spiral phase plate for TE_{11} mode from the profile with the intensity maximum in the center ($n = 0$) forms an asymmetric ring one with two maxima ($n = 1, 2$). For the TE_{01} mode, the initial ring ($n = 0$) structure of the field intensity is transformed into a structure with a maximum radiation intensity in the center ($n = 1$), and later again into a ring ($n = 2$).

The phase front of the beam for the E_y component of the TE_{11} mode changes from spherical to spiral with one on-axis singularity point. Conversely, in the phase profile of the transverse components of the azimuthally polarized TE01 mode, a region with two and three off-axis phase singularity points appears.

ORCID

Andrey V. Degtyarev, https://orcid.org/0000-0003-0844-4282; **Mykola M. Dubinin,** https://orcid.org/0000-0002-7723-9592
Vyacheslav O. Maslov, https://orcid.org/0000-0001-7743-7006; **Konstantin I. Muntean,** https://orcid.org/0000-0001-6479-3511
Oleh O. Svystunov, https://orcid.org/0000-0002-4967-5944

REFERENCES

[1] D. Headland, Y. Monnai, D. Abbott, C. Fumeaux, and W. Withayachumnankul, "Tutorial: Terahertz beamforming, from concepts to realizations", Apl. Photonics, **3**, 051101 (2018). https://doi.org/10.1063/1.5011063
[2] A. Forbes, "Advances in orbital angular momentum lasers", J. Light. Technol., **41**, 2079 (2023). https://doi.org/10.1109/JLT.2022.3220509
[3] H. Wang, Q. Song, Y. Cai, Q. Lin, X. Lu, H. Shangguan, Y. Ai, and S. Xu, "Recent advances in generation of terahertz vortex beams and their applications", Chin. Phys. B, **29**, 097404 (2020). https://doi.org/10.1088/1674-1056/aba2df
[4] N.V. Petrov, B. Sokolenko, M.S. Kulya, A. Gorodetsky, and A.V. Chernykh, "Design of broadband terahertz vector and vortex beams: I. Review of materials and components", Light: Advanced Manufacturing, **3**, 640 (2022). https://doi.org/10.37188/lam.2022.043
[5] T. Nagatsuma, G. Ducournau, and C. Renaud, "Advances in terahertz communications accelerated by photonics", Nat. Photonics, **10**, 371 (2016). https://doi.org/10.1038/nphoton.2016.65
[6] S.C. Chen, Z. Feng, Z., J. Li, W. Tan, L.H. Du, J. Cai, and L.G. Zhu, "Ghost spintronic THz-emitter-array microscope", Light Sci. Appl., **9**, 99 (2020). https://doi.org/10.1038/s41377-020-0338-4
[7] D. Nobahar, S. Khorram, "Terahertz vortex beam propagation through a magnetized plasma-ferrite structure", Opt. Laser Technol., **146**, 107522 (2022). https://doi.org/10.1016/j.optlastec.2021.107522
[8] M.T. Hibberd, A.L. Healy, D.S. Lake, V. Georgiadis, E.J.H. Smith, O.J. Finlay, and S.P. Jamison, "Acceleration of relativistic beams using laser generated terahertz pulses", Nat. Photonics, **14**, 755 (2019). https://doi.org/10.1038/s41566-020-0674-1
[9] A. Klug, I. Nape, and A. Forbes,"The orbital angular momentum of a turbulent atmosphere and its impact on propagating structured light fields", New J. Phys., **23**, 093012 (2021). https://doi.org/10.1088/1367-2630/ac1fca
[10] S.W. Pinnock, S. Roh, T. Biesner, A.V. Pronin, and M. Dressel, "Generation of THz vortex beams and interferometric determination of their topological charge", IEEE Trans. Terahertz Sci. Technol., **13**, 44 (2022). https://doi.org/10.1109/TTHZ.2022.3221369
[11] A. Rubano, F. Cardano, B. Piccirillo, and L. Marrucci, "*Q*-plate technology: a progress review [Invited]", J. Opt. Soc. Am. B, **36,** D70–D87 (2019). https://doi.org/10.1364/JOSAB.36.000D70
[12] R. Imai, N. Kanda, T. Higuchi, K. Konishi, and M. Kuwata-Gonokami, "Generation of broadband terahertz vortex beams", Opt. Lett., **39**, 3714 (2014). https://doi.org/10.1364/OL.39.003714
[13] Y. Yang, X. Ye, L. Niu, K. Wang, Z. Yang, and J. Liu, "Generating terahertz perfect optical vortex beams by diffractive elements", Opt. Express, **28,** 1417 (2020). https://doi.org/10.1364/OE.380076
[14] K. Zhang, Y. Wang, S.N. Burokur, and Q. Wu, "Generating dual-polarized vortex beam by detour phase: from phase gradient metasurfaces to metagratings", IEEE Trans. Microw. Theory Techn., **70**, 200 (2022). https://doi.org/10.1109/TMTT.2021.3075251
[15] X.D. Zhang, Y.H. Su, J.C. Ni, Z.Y. Wang, Y.L. Wang, C.W. Wang, and J.R. Chu, "Optical superimposed vortex beams generated by integrated holographic plates with blazed grating", Appl. Phys. Lett., **111**, 061901 (2017). https://doi.org/10.1063/1.4997590
[16] S.J. Ge, Z.X. Shen, P. Chen, X. Liang, X.K. Wang, W. Hu, Y. Zhang, and Y.Q. Lu, "Generating, separating and polarizing terahertz vortex beams via liquid crystals with gradient-rotation directors", Crystals, **7**, 314 (2017). https://doi.org/10.3390/cryst7100314
[17] S. Guan, J. Cheng, and S. Chang, "Recent progress of terahertz spatial light modulators: materials, principles and applications", Micromachines, **13**, 1637 (2022). https://doi.org/10.3390/mi13101637
[18] A. Al Dhaybi, J. Degert, E. Brasselet, E. Abraham, and E. Freysz, "Terahertz vortex beam generation by infrared vector beam rectification", J. Opt. Soc. Am. B, **36**, 12 (2019). https://doi.org/10.1364/JOSAB.36.000012
[19] K. Miyamoto, K. Sano, T. Miyakawa, H. Niinomi, K. Toyoda, A. Vallés, and T. Omatsu, "Generation of high-quality terahertz OAM mode based on soft-aperture difference frequency generation", Opt. Express, **27**, 31840 (2019). https://doi.org/10.1364/OE.27.031840
[20] H. Sobhani, and E. Dadar, "Terahertz vortex generation methods in rippled and vortex plasmas", J. Opt. Soc. Am. A, **36**, 1187 (2019). https://doi.org/10.1364/JOSAA.36.001187
[21] P. Chevalier, A. Amirzhan, F. Wang, M. Piccardo, S.G. Johnson, F. Capasso, and H.O. Everitt, "Widely tunable compact terahertz gas lasers", Science, **366**, 856 (2019). https://doi.org/10.1126/science.aay8683
[22] J. Farhoomand, and H.M. Pickett, "Stable 1.25 watts CW far infrared laser radiation at the 119 μm methanol line", Int. J. Infrared Millim. Waves, **8**, 441 (1987). https://doi.org/10.1007/BF01013257
[23] H.P. Röser, M. Yamanaka, R. Wattenbach, and G.V. Schultz, "Investigations of optically pumped submillimeter wave laser modes", Int. J. Infrared Millim. Waves, **3**, 839 (1982). https://doi.org/10.1007/BF01008649
[24] M.W. Beijersbergen, R.P.C. Coerwinkel, M. Kristensen, and J.P. Woerdman, "Helical-wavefront laser beams produced with a spiral phase plate", Opt. Commun., **112**, 321 (1994). https://doi.org/10.1016/0030-4018(94)90638-6
[25] V.V. Kotlyar, and A.A. Kovalev, "Nonparaxial propagation of a Gaussian optical vortex with initial radial polarization", J. Opt. Soc. Am. A, **27**, 372 (2010). https://doi.org/10.1364/JOSAA.27.000372
[26] B. Gu, and Y. Cui, "Nonparaxial and paraxial focusing of azimuthal-variant vector beams", Opt. Express, **20**, 17684 (2012). https://doi.org/10.1364/OE.20.017684
[27] Y. Zhang, L. Wang, and C. Zheng, "Vector propagation of radially polarized Gaussian beams diffracted by an axicon", J. Opt. Soc. Am. A, **22**, 2542 (2005). https://doi.org/10.1364/JOSAA.22.002542
[28] O.V. Gurin, A.V. Degtyarev, V.A. Maslov, V.A. Svich, V.M. Tkachenko, and A.N. Topkov, "Selection of transverse modes in laser cavities containing waveguides and open parts", Quantum Electron. **31**, 346 (2001). https://doi.org/10.1070/QE2001v031n04ABEH001949

[29] J.F. Nye, and M.V. Berry, “Dislocations in wave trains”, Proceedings of the Royal Society of London. A. Mathematical and Physical Sciences, **336**, 165 (1974). https://doi.org/10.1098/rspa.1974.0012
[30] O.V. Gurin, A.V. Degtyarev, N.N. Dubinin, M.N. Legenkiy, V.A. Maslov, K.I. Muntean, V.N. Ryabykh, and V.S. Senyuta, “Formation of beams with nonuniform polarisation of radiation in a cw waveguide terahertz laser”, Quantum Electron., **51**, 338 (2021). https://doi.org/10.1070/QEL17511
[31] A.V. Degtyarev, M.M. Dubinin, O.V. Gurin, V.A. Maslov, K.I. Muntean, V.M. Ryabykh, V.S. Senyuta, and O.O. Svystunov, “Control over higher-order transverse modes in a waveguide-based quasi-optical resonator”, Radio Physics and Radio Astronomy, **27**, 129 (2022). https://doi.org/10.15407/rpra27.02.129

ЕВОЛЮЦІЯ ВЕКТОРНИХ ВИХРОВИХ ПРОМЕНІВ, СФОРМОВАНИХ ТЕРАГЕРЦОВИМ ЛАЗЕРНИМ МЕТАЛЕВИМ РЕЗОНАТОРОМ

Андрій В. Дегтярьов, Микола М. Дубінін, Вячеслав О. Маслов, Костянтин І. Мунтян, Олег О. Свистунов
Харківський національний університет імені В.Н. Каразіна, майдан Свободи, 4, Харків, Україна, 61022

Отримано аналітичні вирази для непараксіальної модової дифракції металевого хвилевідного резонатора терагерцового лазера. Дослідження передбачає взаємодію між модами та спіральною фазовою пластиною з урахуванням різних топологічних зарядів (n). Також за допомогою чисельного моделювання досліджено фізичні особливості вихрових пучків, що виникають, коли вони поширюються у вільному просторі. Векторна теорія Релея-Зоммерфельда використовується для дослідження поширення вихрових лазерних променів у зоні Френеля, збуджених модами металевого хвилевідного квазіоптичного резонатора при падінні на спіральну фазову пластину. У вільному просторі спіральна фазова пластина для збуджуючої моди TE_{11} з профілю з максимумом інтенсивності в центрі (n = 0) утворює асиметричне кільце з двома максимумами (n = 1, 2). Для збуджуючої TE_{01} моди початкова поперечна кільцева (n = 0) структура інтенсивності поля трансформується в структуру з максимальною інтенсивністю випромінювання в центрі (n = 1), а потім знову в кільцеву (n = 2). Фазовий фронт променю для E_y компоненти лінійно поляризованої вздовж осі y моди TE_{11} змінюється зі сферичного на спіральний з однією осевою точкою сингулярності, тоді як у фазовому профілі поперечних компонентів азимутально поляризованої моди TE_{01} спостерігається область з двома та та трьома позаосьовими точками сингулярності фази.

Ключові слова: *терагерцовий лазер; металевий хвилевідний резонатор; спіральна фазова пластина; вихрові пучки; поляризація; поширення випромінювання*